Investigating Joint- and Task-Space Impedance Controllers using Baxter Robot

Yinkai Dong [1,2], **Moses C. Nah** [1], **Neville Hogan** [1]

[1]MIT [2]Southern University of Science and Technology

This report investigates the implementation and comparative analysis of joint-space and task-space impedance controllers. These controllers are implemented and tested in MuJoCo simulation using a Baxter robot model. The effectiveness of these controllers is demonstrated with various tasks, e.g., tracking a predetermined trajectory in both joint- and task-spaces, sustaining a constant orientation of the end-effector, managing kinematic singularity and kinematic redundancy of the robot. For managing kinematic singularity, a comparison with operational space control was conducted.

1. Introduction

In this report, we use physics simulation software MuJoCo (Todorov et al., 2012) to delve deep into the application of impedance control (Hogan, 1985; Hogan and Buerger, 2018). This contains a systematic exploration of joint-space and task-space impedance controllers, which are the exemplary examples. For the latter one, implementation on both position and orientation of the end-effector was conducted. With these impedance controllers, the problems of managing kinematic singularity and redundancy are discussed. For the kinematic singularity, the impedance control method was compared with operational space control (Khatib, 1985).

2. Impedance Control — Theory

In this section, we briefly discuss about the theory of impedance control. Given an n-DOF open-chain torque-actuated robotic manipulator, the dynamics is governed by the following equations of motion (Lynch and Park, 2017; Murray et al., 1994):

$$\mathbf{M}(\mathbf{q})\ddot{\mathbf{q}} + \mathbf{C}(\mathbf{q}, \dot{\mathbf{q}})\dot{\mathbf{q}} + \mathbf{g}(\mathbf{q}) = \boldsymbol{\tau}_{in} \tag{1}$$

In this equation, $\mathbf{q} \in \mathbb{R}^{\mathbf{n}}$ is a joint displacement array; $\mathbf{M}(\mathbf{q}) \in \mathbb{R}^{n \times n}$ is the joint-space inertia matrix, which is a symmetric positive-definite matrix for all

$\mathbf{q}$ (Lynch and Park, 2017; Murray et al., 1994); $\mathbf{C}(\mathbf{q}, \dot{\mathbf{q}}) \in \mathbb{R}^{n \times n}$ is the Coriolis/centrifugal matrix; $\mathbf{g}(\mathbf{q}) \in \mathbb{R}^n$ is the vector of gravitational forces; $\boldsymbol{\tau}_{in} \in \mathbb{R}^n$ is the joint-torque input applied by the actuators. Throughout this report, we assume that $\mathbf{g}(\mathbf{q})$ is compensated, i.e., $\mathbf{g}(\mathbf{q})$ on the left-hand side of Eq. 1 can be neglected.

For torque-controlled robots, the goal is to determine the torque input $\boldsymbol{\tau}_{in}$ which produces desired behavior of the robot manipulator. For impedance control, two exemplary methods for designing $\boldsymbol{\tau}_{in}$ are the joint-space and task-space impedance controllers.

2.1. Joint-space Impedance Control

For the joint-space impedance control, $\boldsymbol{\tau}_{in}$ is defined by:

$$\boldsymbol{\tau}_{in} = \mathbf{K}_{\mathbf{q}}(\mathbf{q}_0 - \mathbf{q}) + \mathbf{B}_{\mathbf{q}}(\dot{\mathbf{q}}_0 - \dot{\mathbf{q}}) \tag{2}$$

In this equation, $\mathbf{K}_{\mathbf{q}}, \mathbf{B}_{\mathbf{q}} \in \mathbb{R}^{n \times n}$ are joint-space stiffness and damping matrices; $\mathbf{q}_0 \in \mathbb{R}^n$ is the virtual joint trajectory to which the (virtual) stiffness and damping are connected.

A favorable stability property exists for this controller. If $\mathbf{K}_{\mathbf{q}}, \mathbf{B}_{\mathbf{q}}$ are chosen to be constant positive-definite matrices, and for a fixed $\mathbf{q}_0$, $\mathbf{q}$ asymptotically converges to $\mathbf{q}_0$ (Slotine et al., 1991; Takegaki, 1981).

2.2. Task-Space Impedance Control — Position

For the task-space impedance control, the method can be divided into controlling the position and orientation of the end-effector. For the former one, which we refer to as "position task-space impedance control," $\boldsymbol{\tau}_{in}$ is defined by:

$$\boldsymbol{\tau}_{in} = \mathbf{J}_{\mathbf{p}}(\mathbf{q})^{\mathrm{T}}(\mathbf{K}_{\mathbf{p}}(\mathbf{p}_0 - \mathbf{p}) + \mathbf{B}_{\mathbf{p}}(\dot{\mathbf{p}}_0 - \dot{\mathbf{p}})) \tag{3}$$

In this equation, $\mathbf{K}_{\mathbf{p}}, \mathbf{B}_{\mathbf{p}} \in \mathbb{R}^{3 \times 3}$ are the translational stiffness and damping matrices; $\mathbf{p}_0 \in \mathbb{R}^3$ is the virtual task-space trajectory to which the (virtual) stiffness and damping are connected; $\mathbf{p} = \mathbf{p}(\mathbf{q}) \in \mathbb{R}^3$ is the end-effector position of the robot at joint configuration $\mathbf{q}$; $\mathbf{J}_{\mathbf{p}}(\mathbf{q}) \in \mathbb{R}^{3 \times n}$ is the linear velocity part of the Jacobian matrix (Siciliano et al., 2008), which is derived by taking the partial derivatives of $\mathbf{p}(\mathbf{q})$ with respect to $\mathbf{q}$, i.e., $\mathbf{J}_{\mathbf{p}}(\mathbf{q}) = \partial \mathbf{p}(\mathbf{q}) / \partial \mathbf{q}$.*
As with the joint-space impedance controller (Section 2.1), a favorable stability property exists for this controller. For constant positive definite $\mathbf{K}_{\mathbf{p}}, \mathbf{B}_{\mathbf{p}}$ matrices, and for a constant $\mathbf{p}_0$, $\mathbf{p}$ asymptotically converges to $\mathbf{p}_0$ (Takegaki, 1981).

*This also implies that $\dot{\mathbf{p}} = \mathbf{J}_{\mathbf{p}}(\mathbf{q})\dot{\mathbf{q}}$.

2.3. Task-Space Impedance Control — Orientation

Along with the position task-space impedance control, orientation task-space impedance control makes the current end-effector's orientation converge to the desired orientation. In detail, given a fixed inertial frame $\{0\}$, let the current and desired orientation be denoted as ${}^0\mathbf{R}_c$ and ${}^0\mathbf{R}_d$, where ${}^0\mathbf{R}_c$ (respectively ${}^0\mathbf{R}_d$) is an element of the Special Orthogonal group SO(3) (Lynch and Park, 2017; Murray et al., 1994) and describes the orientation of the current (respectively desired) frame with respect to $\{0\}$.
The orientation task-space impedance controller is defined by (Hermus et al., 2021):

$$\boldsymbol{\tau}_{in} = \mathbf{J}_{\omega}^{\mathrm{T}}(\mathbf{q})(k_e\theta\, {}^0\boldsymbol{\epsilon} - b_e\boldsymbol{\omega}) \tag{4}$$

In this equation, ${}^0\boldsymbol{\epsilon} \in \mathbb{R}^3$ and $\theta \in [0, \pi)$ correspond to the elements of the axis-angle notation (Lynch and Park, 2017) of ${}^c\mathbf{R}_d = {}^0\mathbf{R}_c^T\, {}^0\mathbf{R}_d$, respectively; superscript 0 is used to emphasize that the axis is expressed with respect to $\{0\}$; $k_e, b_e \in \mathbb{R}$ are positive scalar values which correspond to the rotational stiffness and damping attached to axis ${}^0\boldsymbol{\epsilon}$, respectively; $\boldsymbol{\omega} \in \mathbb{R}^3$ is the angular velocity of the end-effector; $\mathbf{J}_{\omega}(\mathbf{q}) \in \mathbb{R}^{3\times n}$ is the angular velocity part of the Jacobian matrix, i.e., $\boldsymbol{\omega} = \mathbf{J}_{\omega}(\mathbf{q})\dot{\mathbf{q}}$ (Siciliano et al., 2008).

2.4. Superposition Principle of Mechanical Impedances

Even though each of the equation of the impedance controller is a nonlinear operator, these controllers can be "linearly " superimposed (Hogan, 1985). This is the "superposition principle" of mechanical impedances, which can be expressed as:

$$\boldsymbol{\tau}_{in} = \sum_{i=1}^{n} \boldsymbol{\tau}_{in,i} \tag{5}$$

In this equation, $\boldsymbol{\tau}_{in,i}$ is the i-th impedance controller which is superimposed. While different types of impedance controllers other than Eq. 2, 3, 4 can be used, in this report we focus on using Eq. 2, 3, 4 as the basic element of the impedance controller.
The superposition principle of mechanical impedances plays a crucial role to solve multiple tasks, e.g., managing kinematic redundancy and singularity of the robotic manipulator. The details are presented in the next section.

3. Simulation with Baxter Robot

In this section, we show the implementation of multiple impedance controllers in simulation (Section 2). For the implementation, we use MuJoCo simulator (Todorov et al., 2012) and Baxter robot model.

3.1. Model of Baxter Robot

The Baxter robot, developed by Rethink Robotics is a dual-arm robot. Each arm has 7-DOF (Figure **1**). For each joint of the robot, (ideal) torque actuators are mounted. Since Baxter robot already contains a low-level gravity compensation controller, gravity was set to be a zero vector in the simulation.

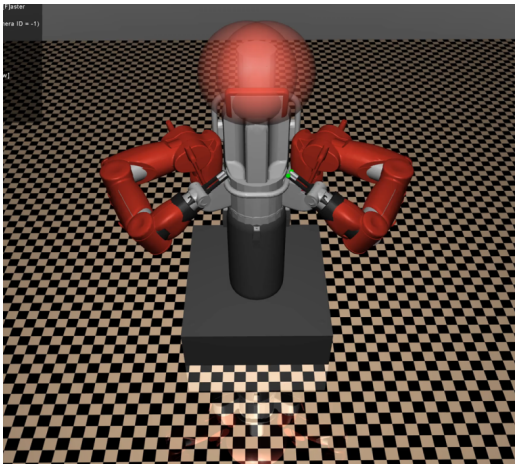

Fig. 1: MuJoCo model of Baxter Robot.

3.2. Implementation of Joint-space Impedance Control

For both arms of the Baxter robot, a joint-space impedance controller (Eq. 2) was implemented. For the virtual joint trajectory $\mathbf{q}_0(t)$, the minimum-jerk trajectory (Flash, 1987; Hogan and Flash, 1987) was used:

$$\mathbf{q}_0(t) = \begin{cases} \mathbf{q}_{0,i} & t < t_0 \\ \mathbf{q}_{0,i} + (\mathbf{q}_{0,f} - \mathbf{q}_{0,i}) \left[10 \cdot \left(\frac{t-t_0}{D}\right)^3 - 15 \cdot \left(\frac{t-t_0}{D}\right)^4 + 6 \cdot \left(\frac{t-t_0}{D}\right)^5 \right] & t_0 \leq t < t_0 + D \\ \mathbf{q}_{0,f} & t_0 + D \leq t \end{cases} \tag{6}$$

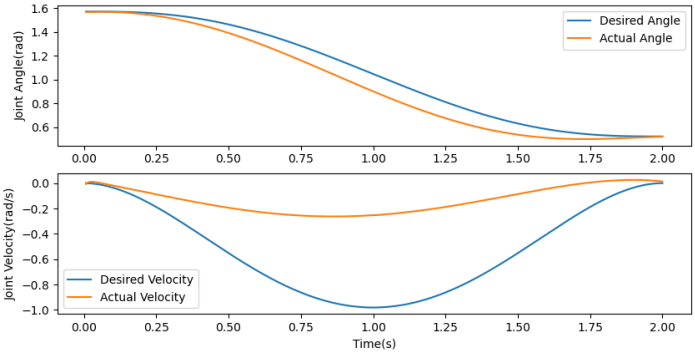

Fig. 2: Virtual trajectory and actual trajectory of the elbow-joint with joint-space impedance control. The initial joint angle for the right hand and left hand are $\mathbf{q}_{0,i,r}$ = [-0.314, 0.1, 1.571, 1.571, 0.393, 1.571, -1.571], $\mathbf{q}_{0,i,l}$ = [0.314, 0.1, -1.571, 1.571, -0.393, 1.571, 1.571]. The final joint angle for the right hand and left hand are $\mathbf{q}_{0,f,r}$ = [-0.105, 0.033, 0.524, 0.524, 0.131, 0.524, -0.524], $\mathbf{q}_{0,f,l}$ = [0.105, 0.033, -0.524, 0.524, -0.131, 0.524, 0.524]. For the plot the second wrist joint, which is the sixth joint of the right/left arm, was chosen. $\mathbf{K_q} = 50\mathbf{I}_7$, $\mathbf{B_q} = 10\mathbf{I}_7$ where $\mathbf{I}_7 \in \mathbb{R}^{7\times7}$ is an identity matrix.

In this equation, $\mathbf{q}_{0,i}, \mathbf{q}_{0,f} \in \mathbb{R}^n$ correspond to the initial, final (virtual) joint posture, respectively; D is the duration of the movement; t_0 is the starting time of the trajectory.

Given the minimum-jerk trajectory as input to each joint, the comparison of the virtual $\mathbf{q}_0(t)$ and actual $\mathbf{q}(t)$ joint trajectories is shown in Figure **2**. The result shows that $\mathbf{q}(t)$ eventually converges to the final (virtual) joint posture $\mathbf{q}_{0,f}$.

3.3. Implementation of Task-Space Impedance Control — The Problem of Kinematic Redundancy

For both arms of the Baxter robot, position task-space impedance controller (Eq. 3) was implemented. For $\mathbf{p}_0(t)$, a circular trajectory was used:

$$\mathbf{p}_0(t) = \begin{bmatrix} r_x \\ r_y + r_0\cos(\omega t + \phi) \\ r_z + r_0\sin(\omega t + \phi) \end{bmatrix} \tag{7}$$

The simulation result of the actual joint angle and velocity is shown in Figure **3** (**a**), and the Cartesian position of the end-effector is shown in Figure **3** (**b**).

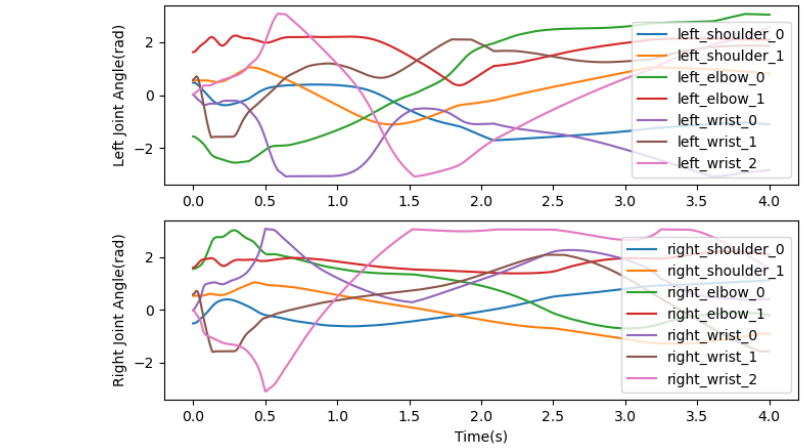

(**a**)

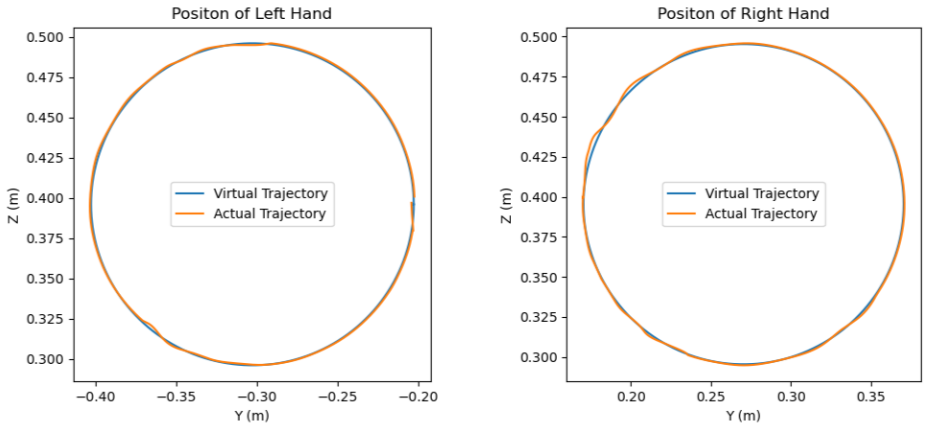

(**b**) (**c**)

Fig. 3: (**a**) Joint-space trajectory of one of the Baxter robot arms using position task-space impedance control. (**b**) Cartesian position of the left hand, (**c**) Cartesian position of the right hand. $\mathbf{K_p} = 500\mathbf{I}_3$, $\mathbf{B_p} = 10\mathbf{I}_3$. The parameters of the circular trajectory (Eq. 7) used for $\mathbf{p}_0(t)$: r_x = 0.75 m, r_y = -0.30 m, r_z = 0.30 m, r_0 = 0.10 m, $\omega = \pi$ rad/s, $\phi = 0$ rad. The initial joint angle for the right hand and left hand are $\mathbf{q}_{0,l}$ = [0.467, 0.542, -1.560, 1.618, 0.012, 0.575, 0.023] rad, $\mathbf{q}_{0,r}$ = [-0.511, 0.538, 1.561, 1.609, -0.009, 0.590, -0.017] rad.

The resulting Cartesian-space trajectory of the end-effector is (almost) a circle. It is suspected that perfect tracking was not achieved due to the joint limit of the Baxter robot defined in the MuJoCo model. As shown in the joint trajec-

tory Figure **3** (**a**), because of the kinematic redundancy of the Baxter robot, (i.e., for a 7-DOF arm with a 3-dimensional task, there is a 4-dimensional kinematic redundancy), an undesired motion in the joint-space occurs.

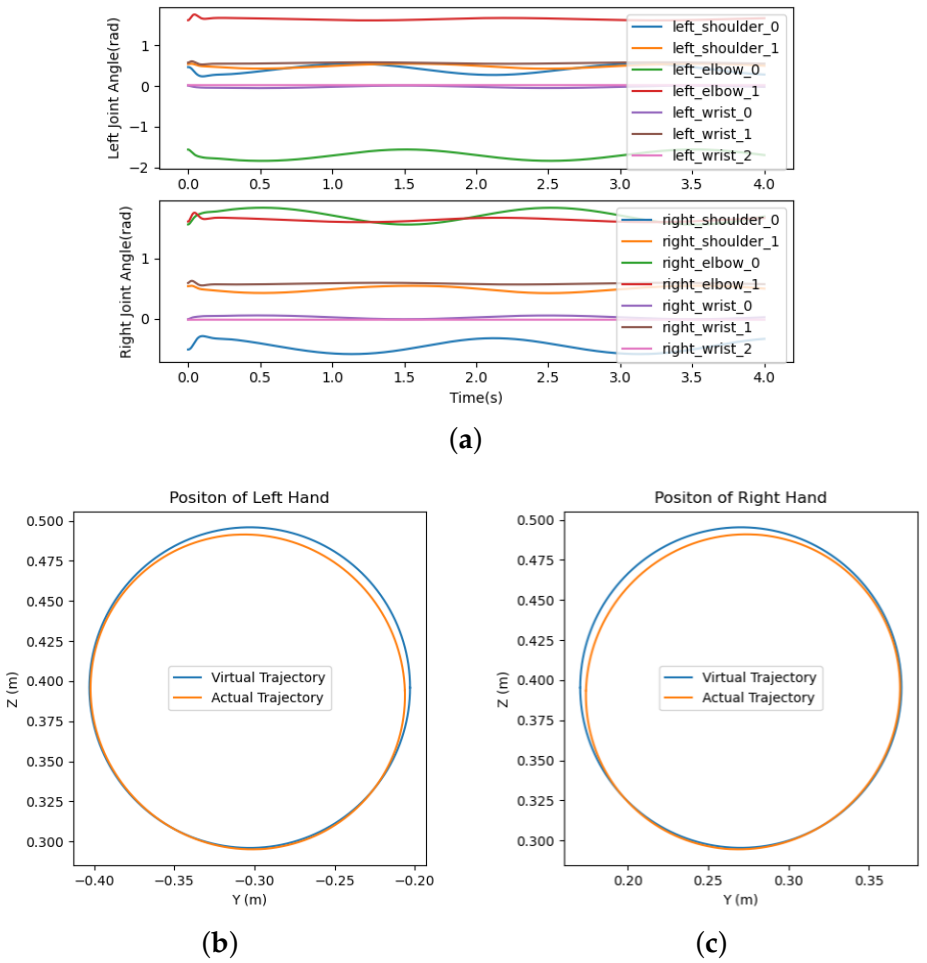

Fig. 4: (**a**) Joint-space trajectory, (**b**) Cartesian position of the left hand, and (**b**) Cartesian position of the left hand. Controller parameters: $\mathbf{K_q} = 5\mathbf{I}_7$, $\mathbf{B_q} = 7\mathbf{I}_7$, $\mathbf{K_p} = 60\mathbf{I}_3$, $\mathbf{B_q} = 10\mathbf{I}_3$. The initial joint angle for the right hand and left hand are $\mathbf{q}_{0,l}$ = [0.467, 0.542, -1.560, 1.618, 0.012, 0.575, 0.023] *rad*, $\mathbf{q}_{0,r}$ = [-0.511, 0.538, 1.561, 1.609, -0.009, 0.590, -0.017] *rad*. These initial joint angles were the virtual joint posture of the joint-space impedance controller.

3.4. Managing Kinematic Redundancy with Impedance Superposition

3.4.1. Task-space and Joint-space Impedance Control

To manage the kinematic redundancy of the robot, a joint-space impedance controller (Eq. 2) is superimposed to the position task-space impedance controller (Eq. 3) (Figure **4**).

The results showed that after superimposing two impedance controllers, the angular trajectory of each joint became smoother, and the kinematic redundancy of the robot is managed. However, as shown in Figure **4** (**b, c**), task conflict exists between the two impedance controller, which thereby increases the tracking error in Cartesian space (Figure **4**).

3.4.2. Orientation Task-space Impedance Control

The task of tracking a task-space trajectory while maintaining a specific orientation was implemented. Each hand of the Baxter robot is given a pre-determined orientation and virtual trajectory planned in task-space, as shown in Figure **5**. The virtual trajectory of the right (respectively left) hand is a triangle (respectively square).

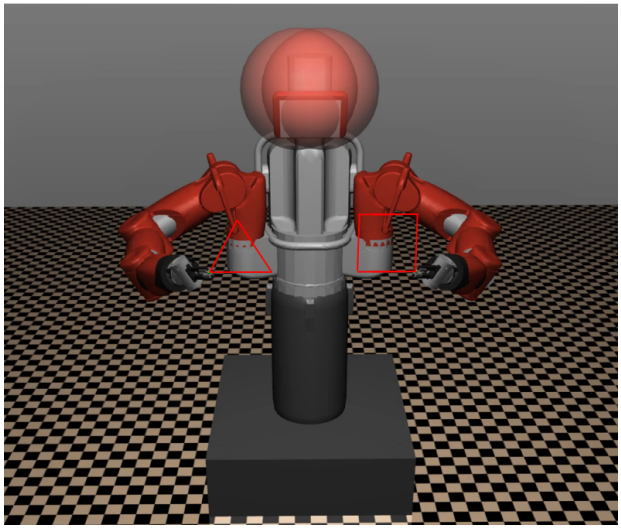

Fig. 5: Simulation posture of Baxter Robot and the virtual task-space trajectory of both arms.

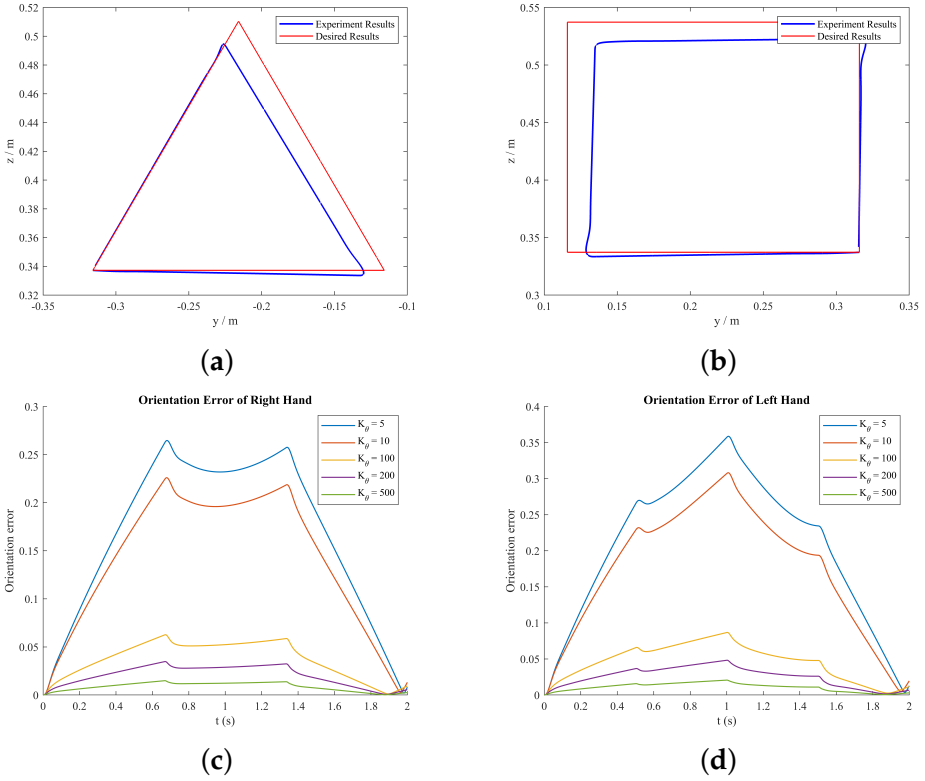

Fig. 6: The resulting end-effector trajectory for (**a**) triangle and (**b**) square virtual trajectories. Parameters: $\mathbf{K_q} = 200\mathbf{I}_7$, $\mathbf{B_q} = 5\mathbf{I}_7$, $\mathbf{K_p} = 5\mathbf{I}_3$, $\mathbf{B_q} = 7\mathbf{I}_3$, $k_\theta = 5$, $b_\theta = 7$. (**c**) Orientation error of right hand. (**d**) Orientation error of left hand. The right-hand trajectory is represented by a triangle of length 0.2 in YZ Plane, starting at point $\mathbf{p_{0,r}} = [0.84, -0.32, 0.34]m$. The trajectory of the left hand is represented by a square of length 0.2 in YZ Plane, starting at point $\mathbf{p_{0,l}} = [0.84, 0.32, 0.34]m$. The initial joint angle for the right hand and left hand are: $\mathbf{q}_{0,r}$ = [-0.628, 0.524, 1.571, 1.571, 0, 0.628, 0] rad, $\mathbf{q}_{0,l}$ = [0.628, 0.524, -1.571, 1.571, 0, 0.628, 0] rad, respectively.

The results are shown in Figure **6**. Deviations from the task-space trajectory are observed when the end-effector moves away from the initial points $\mathbf{p_{0,r}}$ and $\mathbf{p_{0,l}}$, shown in Figure **6** (**a, b**). These deviations can be attributed to the influence between virtual stiffness and damping of multiple impedance controllers. The orientation error is calculated by the Frobenius norm of the difference between the current and desired orientation matrices ${}^{\mathbf{0}}\mathbf{R}_{\mathbf{c}}^{\mathbf{T}}\ {}^{\mathbf{0}}\mathbf{R}_{\mathbf{d}} - \mathbf{I}_3$ over time, shown in Figure **6 (c, d)**. The orientation error is small when approaching the initial point $\mathbf{p_{0,r}}$ and $\mathbf{p_{0,l}}$, and as the orientation virtual stiffness k_θ increases, the overall error decreases.

3.5. Managing Kinematic Singularity — A Comparison with Operational Space Control

We show how the robot's behavior near kinematic singularity can be managed using impedance control. For this, a comparison of performance with Operational Space Control (Khatib, 1985) was conducted. For the Operational Space Control, the following controller input was used (Khatib, 1985):

$$\boldsymbol{\tau}_{in} = \mathbf{J}(\mathbf{q})^{\mathbf{T}} \cdot \mathbf{F_{in}} \tag{8}$$

where:

$$\begin{aligned}
\mathbf{F}_{in} &= \mathbf{F}'_{in} + \mathbf{F}^{*}_{in} \\
\mathbf{F}^{*}_{in} &= \boldsymbol{\Lambda}(\mathbf{q})\{-\mathbf{b}^{*} - \dot{\mathbf{J}}(\mathbf{q})\,\dot{\mathbf{q}}\} \\
\boldsymbol{\Lambda}(\mathbf{q}) &= (\mathbf{J}(\mathbf{q})\mathbf{M}^{-\mathbf{1}}(\mathbf{q})\mathbf{J}(\mathbf{q})^{\mathbf{T}})^{-\mathbf{1}} \\
\mathbf{b}^{*} &= -\mathbf{J}(\mathbf{q})\,\mathbf{M}^{-1}(\mathbf{q})\mathbf{C}(\mathbf{q},\dot{\mathbf{q}})\dot{\mathbf{q}} - \mathbf{J}(\mathbf{q})\,\mathbf{M}^{-1}(\mathbf{q})\mathbf{g}(\mathbf{q}) \\
\mathbf{F}'_{in} &= \boldsymbol{\Lambda}(\mathbf{q})\{\ddot{\mathbf{p}}_0 + \mathbf{K_o}\,(\mathbf{p}_0 - \mathbf{p}) + \mathbf{B}_o\,(\dot{\mathbf{p}}_0 - \dot{\mathbf{p}})\}
\end{aligned}$$

In these equations, $\mathbf{K_o}$ is the stiffness matrix of the operational space control, $\mathbf{B_o}$ is the damping matrix of the operational space control, $\boldsymbol{\Lambda}(\mathbf{q})$ is the generalized moment of inertia" matrix (Asada, 1983), which is the inverse of the "end-point mobility tensor" (Hogan, 1985).

We forced the robot's end-effector to reach near kinematic singularity, by controlling $\mathbf{p_0}(t)$ of the position task-space impedance controller (Eq. 3) and operational space control (Eq. 8). In detail, $\mathbf{p_0}(t)$ was chosen to be a minimum-jerk trajectory, and the final Cartesian position of the trajectory was set to be sufficiently outside the reachable workspace of the robot. This eventually "straightens" the robot manipulator and consequently leads to a kinematic singularity.
For Operational Space Control, when the robot's end-effector approaches near kinematic singularity (i.e., the Jacobian matrix becomes rank-deficit), the generalized moment of inertia becomes unbounded. Consequently, the control input is unbounded, which thereby causes the robot to be unstable near the kinematic singularity. This behavior is an inevitable constraint of Operational Space Control, dictated by the mathematical characteristics of the controller design (Figure **7** (**a**)-(**c**)).

On the other hand, superimposing multiple impedance controllers manages kinematic singular without introducing instability. This is due to the fact that an inverse of the Jacobian matrix is not required for the task-space impedance controller (Figure **7** (**d**)-(**f**)).

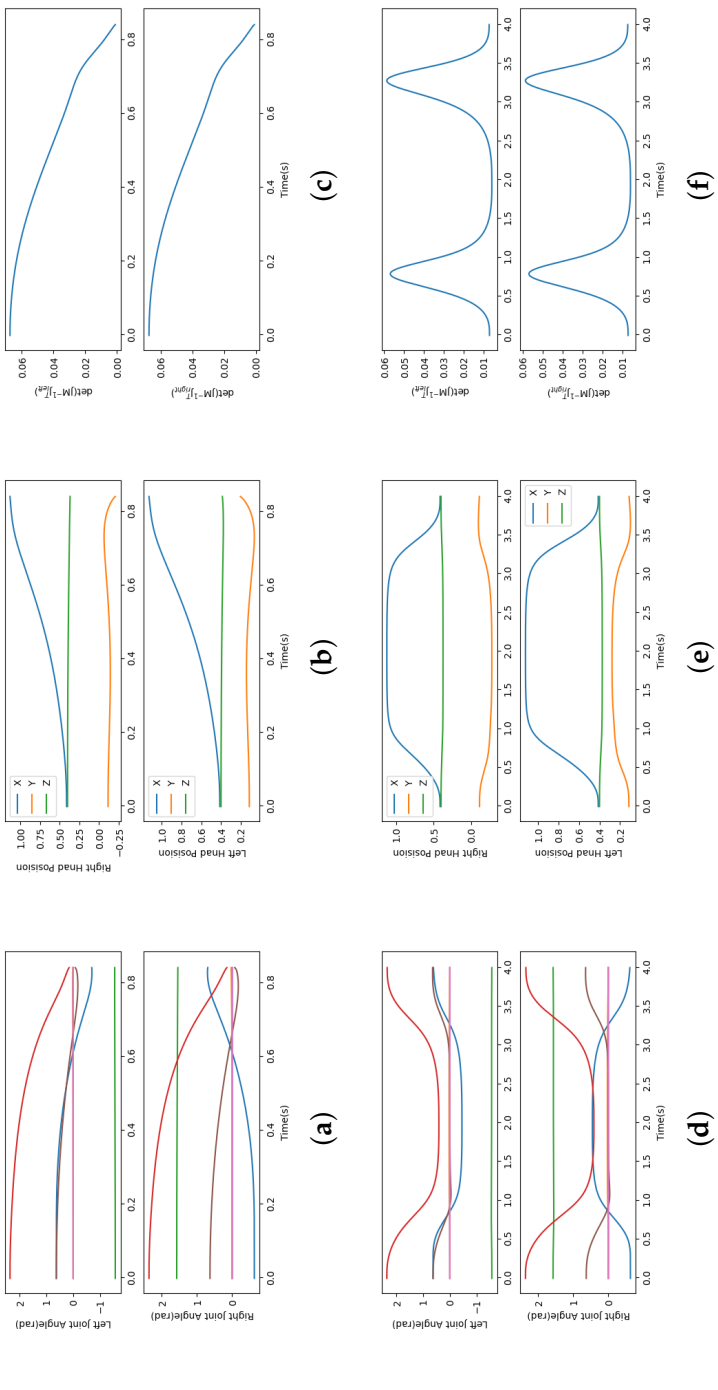

Fig. 7: Simulation trajectory with Operational Space control for (**a**) Joint-space trajectory, (**b**) end-effector Cartesian trajectory, and (**c**) the determinant of $\mathbf{\Lambda}^{-1}(\mathbf{q})$. Parameters: $\mathbf{K}_o = 50\mathbf{I}_7$, $\mathbf{B}_o = 7\mathbf{I}_7$. Simulation trajectory with task-space and joint-space impedance controls. (**d**) joint-space trajectory, (**e**) end-effector Cartesian trajectory, and (**f**) the determinant of $\mathbf{\Lambda}^{-1}(\mathbf{q})$. Parameters: $\mathbf{K_q} = 100\mathbf{I}_7$, $\mathbf{B_q} = 7\mathbf{I}_7$, $\mathbf{K_p} = 5\mathbf{I}_3$, $\mathbf{B_q} = 7\mathbf{I}_3$.

3.6. The Problem of Repeatability

For kinematically redundant robots, it is well known that the repeating motion in task-space produces a non-negligible drift in joint-space trajectories (Klein and Huang, 1983). In other words, given an end-effector position $\mathbf{p}$, there exists an infinite number of solutions for $\mathbf{q}$ which produce the same $\mathbf{p} = \mathbf{f}(\mathbf{q})$. This problem of repeatability (or integrability) (Mussa-Ivaldi and Hogan, 1991) can be addressed with impedance controller, where for a given $\mathbf{p}$, there exists a unique $\mathbf{q}$, hence the map from $\mathbf{p}$ to $\mathbf{q}$ is well-defined.

To explore the performance of repeatability using impedance control, we use the same trajectory of the position task-space impedance control in Section 3.4.1, Eq. 7 and repeat the circle trajectory multiple times, as shown in Figure **8**. The findings indicate that the robot system's motion under impedance control exhibits a high level of repeatability in both joint- and task-space trajectories.

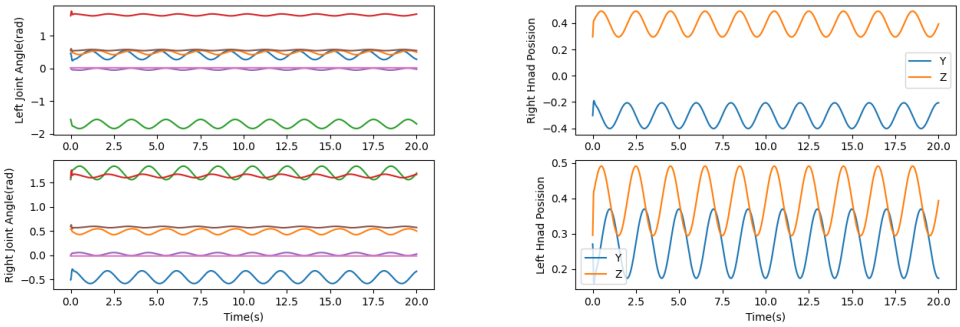

(**a**) (**b**)

Fig. 8: Simulation with Impedance Control. (**a**) Joint-space trajectory and (b) end-effector Cartesian trajectory. Parameters: $\mathbf{K_q} = 5\mathbf{I}_7$, $\mathbf{B_q} = 7\mathbf{I}_7$, $\mathbf{K_p} = 500\mathbf{I}_3$, $\mathbf{B_q} = 10\mathbf{I}_3$.

4. Conclusion

In conclusion, this study presents an in-depth exploration and comparison of various impedance controllers: joint-space impedance control and task-space impedance control. Simulations using Baxter Robot demonstrate the effectiveness of these impedance controllers for multiple tasks. For instance, we show that tracking a predetermined trajectory in both joint- and task-spaces, sustaining a constant orientation of the end-effector, and managing kinematic singular-

ity and kinematic redundancy of the robot can be achieved with impedance controllers. Overall, the findings affirm the practicality and potential of impedance controllers in multiple robotic applications.

References

Asada H (1983) A geometrical representation of manipulator dynamics and its application to arm design. *Journal of dynamic systems, measurement, and control* 105(3): 131–142.

Flash T (1987) The control of hand equilibrium trajectories in multi-joint arm movements. *Biological cybernetics* 57(4): 257–274.

Hermus J, Lachner J, Verdi D and Hogan N (2021) Exploiting redundancy to facilitate physical interaction. *IEEE Transactions on Robotics* 38(1): 599–615.

Hogan N (1985) Impedance control-an approach to manipulation. i-theory. ii-implementation. iii-applications. *ASME Journal of Dynamic Systems and Measurement Control B* 107: 1–24.

Hogan N and Buerger SP (2018) Impedance and interaction control. In: *Robotics and automation handbook*. CRC press, pp. 375–398.

Hogan N and Flash T (1987) Moving gracefully: quantitative theories of motor coordination. *Trends in neurosciences* 10(4): 170–174.

Khatib O (1985) Real-time obstacle avoidance for manipulators and mobile robots. In: *Proceedings. 1985 IEEE International Conference on Robotics and Automation*, volume 2. IEEE, pp. 500–505.

Klein CA and Huang CH (1983) Review of pseudoinverse control for use with kinematically redundant manipulators. *IEEE Transactions on Systems, Man, and Cybernetics* : 245–250.

Lynch KM and Park FC (2017) *Modern robotics*. Cambridge University Press.

Murray RM, Sastry SS and Zexiang L (1994) A mathematical introduction to robotic manipulation.

Mussa-Ivaldi FA and Hogan N (1991) Integrable solutions of kinematic redundancy via impedance control. *The International Journal of Robotics Research* 10(5): 481–491.

Siciliano B, Khatib O and Kröger T (2008) *Springer handbook of robotics*, volume 200. Springer.

Slotine JJE, Li W et al. (1991) *Applied nonlinear control*. Prentice hall Englewood Cliffs, NJ.

Takegaki M (1981) A new feedback method for dynamic control of manipulators. *Trans. ASME, Ser. G, J. Dynamic Systems, Measurement, and Control* 103(2): 119–125.

Todorov E, Erez T and Tassa Y (2012) Mujoco: A physics engine for model-based control. In: *2012 IEEE/RSJ international conference on intelligent robots and systems*. IEEE, pp. 5026–5033.